The Journal of Immunology

Rab11-FIP3 Regulation of Lck Endosomal Traffic Controls TCR Signal Transduction

Jérôme Bouchet, Iratxe del Río-Iñiguez, Elena Vázquez-Chávez, Rémi Lasserre, Sonia Agüera-González, Céline Cuche, Mary W. McCaffrey, Vincenzo Di Bartolo and Andrés Alcover

J Immunol 2017; 198:2967-2978; Prepublished online 24 February 2017;
doi: 10.4049/jimmunol.1600671
http://www.jimmunol.org/content/198/7/2967

The Journal of Immunology is published twice each month by
The American Association of Immunologists, Inc.,
1451 Rockville Pike, Suite 650, Rockville, MD 20852

Print ISSN: 0022-1767 Online ISSN: 1550-6606.

Rab11-FIP3 Regulation of Lck Endosomal Traffic Controls TCR Signal Transduction

Jérôme Bouchet,*,†,‡,[1] Iratxe del Río-Iñiguez,*,†,‡ Elena Vázquez-Chávez,*,†,‡ Rémi Lasserre,*,†,[2] Sonia Agüera-González,*,†,[3] Céline Cuche,*,†,‡ Mary W. McCaffrey,[§] Vincenzo Di Bartolo,*,†,‡ and Andrés Alcover*,†,‡

The role of endosomes in receptor signal transduction is a long-standing question, which remains largely unanswered. The T cell Ag receptor and various components of its proximal signaling machinery are associated with distinct endosomal compartments, but how endosomal traffic affects T cell signaling remains ill-defined. In this article, we demonstrate in human T cells that the subcellular localization and function of the protein tyrosine kinase Lck depends on the Rab11 effector FIP3 (Rab11 family interacting protein-3). FIP3 overexpression or silencing and its ability to interact with Rab11 modify Lck subcellular localization and its delivery to the immunological synapse. Importantly, FIP3-dependent Lck localization controls early TCR signaling events, such as tyrosine phosphorylation of TCRζ, ZAP70, and LAT and intracellular calcium concentration, as well as IL-2 gene expression. Interestingly, FIP3 controls both steady-state and poststimulation phosphotyrosine and calcium levels. Finally, our findings indicate that FIP3 modulates TCR-CD3 cell surface expression via the regulation of steady-state Lck-mediated TCRζ phosphorylation, which in turn controls TCRζ protein levels. This may influence long-term T cell activation in response to TCR-CD3 stimulation. Therefore, our data underscore the importance of finely regulated endosomal traffic in TCR signal transduction and T cell activation leading to IL-2 production. *The Journal of Immunology*, **2017, 198: 2967–2978.**

Adaptive immune responses are initiated within lymphoid organs when circulating T lymphocytes recognize Ags displayed on the surface of APCs. T cell Ag receptors recognize molecular fragments, often peptides (peptide Ag), associated with MHC molecules expressed on the surface of APCs. The TCR is a complex of six polypeptides termed TCR-CD3, which recognizes Ag-MHC, through its TCRαβ subunits, and transduces activation signals through the CD3γ, CD3δ, CD3ε and TCRζ subunits. CD3γ, CD3δ, CD3ε and TCRζ subunits contain in their intracellular regions ITAMs that are phosphorylated immediately after TCR engagement. ITAM phosphorylation of the TCRζ subunit by the Src family protein tyrosine kinases Lck and Fyn allows the recruitment of the Syk family tyrosine kinase ZAP70kDa via its SH2 domains. ZAP70 recruitment facilitates its tyrosine phosphorylation and activation, and the subsequent tyrosine phosphorylation of signaling adapters, including LAT and SLP76. Adapter phosphorylation mediates the recruitment of several signaling effector molecules forming an amplification signalosome necessary to proceed to downstream activation events. These events involve the activation of several serine-threonine kinases, including MAPK, which lead to NFAT, NF-κB, and AP-1 transcription factor activation. Altogether, these T cell signaling cascades drive T cell growth, differentiation, and production of cytokines, crucial for the development of adaptive immune responses (1).

TCR signal transduction is initiated and regulated at the immunological synapse, an organized junction between T cells and APCs (2). Immunological synapses concentrate TCR-CD3 and

*Department of Immunology, Lymphocyte Cell Biology Unit, Institut Pasteur, 75724 Paris, France; †CNRS URA1961, 75724 Paris Cedex 15, France; ‡INSERM U1221, 75724 Paris Cedex 15, France; and §Molecular Cell Biology Laboratory, School of Biochemistry and Cell Biology, Biosciences Institute, University College Cork, Cork, Ireland

[1]Current address: Institut Cochin INSERM, U1016, CNRS, UMR8104, Université Paris Descartes, Sorbonne Paris Cité, Paris, France.

[2]Current address: Centre d'Immunologie de Marseille Luminy, Université Aix-Marseille, CNRS UMR7280, INSERM U1104, Marseille, France.

[3]Current address: Membrane and Cytoskeleton Dynamics Group, Institut Curie, CNRS UMR144, Paris, France.

ORCIDs: 0000-0002-6611-4380 (J.B.); 0000-0002-9461-1608 (E.V.-C.); 0000-0002-5453-947X (V.D.B.); 0000-0002-9507-3450 (A.A.).

Received for publication April 18, 2016. Accepted for publication January 27, 2017.

This work was supported by grants from the Agence Nationale de Recherche (ANR; Grant 11 BSV3 025 01), the ANR sur le SIDA et les Hepatitis Virales (Grant AO 2013-02 CSS1 No 1339/14673), the Institut Pasteur, CNRS, INSERM, and the People Programme (Marie Sklodowska-Curie Actions) of the European Union's Seventh Framework Programme (Grant FP7/2007-2013) under the Research Executive Agency Grant agreement 317057 HOMIN-ITN (to A.A.), and by Science Foundation Ireland Principal Investigator Award 09/IN.1/B2629 (to M.W.M.). The Imagopole is part of the France BioImaging infrastructure supported by Grant ANR-10-INSB-04-01, "Investments for the Future." Personnel funding was as follows: ANR sur le SIDA et les Hepatitis Virales and Roux-Institut Pasteur postdoctoral funding to J.B.; European Union Marie Curie Actions HOMIN-ITN (cited earlier) predoctoral funding to I.d.R.-I., who is a scholar in the Pasteur-Paris University International Ph.D. program; Roux-Institut Pasteur and ANR postdoctoral funding to R.L.; Fondation ARC pour la Recherche sur le Cancer and ANR postdoctoral funding to S.A.-G.; and ANR and Sidaction postdoctoral funding to E.V.-C.

J.B. designed the project, designed and performed the experiments, analyzed the data, and contributed to writing the manuscript; I.d.R.-I. performed experiments, analyzed and discussed data, and critically commented on the manuscript; E.V.-C. designed, performed, analyzed and discussed experiments, and contributed to writing the manuscript; R.L., S.A.-G., and V.D.B. provided expertise, contributed to data analyses and discussions, and critically commented on the manuscript; C.C. provided technical and organizational support; M.W.M. provided expression vectors, previous expertise, and critical reading of the manuscript; A.A. conceived the project, contributed to data analyses and discussions, and wrote the manuscript.

Address correspondence and reprint requests to Prof. Andrés Alcover and Dr. Jérôme Bouchet, Institut Pasteur, Unité de Biologie Cellulaire des Lymphocytes, 28 Rue du Dr Roux, 75724 Paris, France. E-mail addresses: andres.alcover@pasteur.fr (A.A.) and jerome.bouchet@inserm.fr (J.B.)

Abbreviations used in this article: ANR, Agence Nationale de Recherche; ERC, endosomal recycling compartment; FIP3, Rab11 family interacting protein-3; ICAReB, Institut Pasteur Clinical Investigation and Access to Biological Resources; IFT, intraflagellar transport protein; PDBu, phorbol 12,13-dibutyrate; RT-qPCR, retrotranscription quantitative PCR; siRNA, small interfering RNA; WT, wild type.

signaling molecules, including Lck, ZAP70, LAT, and SLP76, forming dynamic microclusters critical to regulate downstream signaling. Moreover, costimulatory receptors, like CD28, and adhesion molecules, like LFA1, also cluster at the immunological synapse. Immunological synapse formation and T cell activation results from a T cell polarization process that requires the orchestrated action of the actin and microtubule cytoskeleton and of intracellular vesicle traffic (2, 3).

To cluster at the immunological synapse, TCR and signaling molecules need to be transported to the synapse and/or retained there. Although the LFA1 integrin was shown to be transported via the plasma membrane by myosin molecular motors (4), several endosomal compartments, expressing distinct vesicle traffic regulators, deliver TCR subunits, Lck and LAT, to the immunological synapse (5–19). Thus, Lck was shown to be associated with vesicles displaying Rab11 (12), the transport protein MAL (13), and Unc119 (14); TCRζ traffic is associated with Rab4, Rab8, and Rab35 vesicles, the microtubule-associated protein EB1, the SNAREs proteins VAMP3 and VAMP7, and intraflagellar transport proteins (IFTs) (12, 15–17, 19); and LAT is associated with vesicles displaying Rab7, Rab27, Rab37, VAMP7, and IFTs (11, 12, 18). Consistent with the differential compartment association, the delivery of these various signaling proteins to the immunological synapse is differentially regulated. Thus, LAT is delivered to the synapse in an intracellular calcium-, synaptotagmin-7–, VAMP7-, and IFT20-dependent fashion (11, 12, 18), whereas Lck delivery depends on MAL and Unc119 (12–14). Importantly, blocking the delivery to the synapse of vesicles carrying Lck or LAT inhibited the generation of signaling complexes at the synapse and downstream effects leading to cytokine production (8, 11–14, 18).

Endosomal traffic is regulated by a variety of Rab GTPases (20). Among them, Rab11 controls trafficking through the endosomal recycling compartment (ERC), a key organelle involved in "long loop" endosomal recycling of receptors, their storage, and in transcytosis (21). The Rab11 ERC is built around the centrosome in a microtubule-dependent manner. Rab11 regulates the transport and localization of a variety of cell surface receptors and adhesion proteins through the ERC. Moreover, Rab11 influences various cellular processes, including ciliogenesis, neuritogenesis, cytokinesis, and cell polarity (22). Rab11 function is tightly related with that of the exocyst complex, a multisubunit protein complex involved in tethering secretory vesicles to the plasma membrane (21–23). Rab11-mediated vesicle traffic depends on a number of effector proteins that include the Rab11 family interacting proteins (FIPs; also known as Rab11-FIPs), Rabphilin-11/Rab11BP, myosin-V, phosphoinositide 4-kinase-β, and the exocyst complex protein Sec15 (24). FIPs are an evolutionarily conserved family of proteins that act as effectors of Rab11, as well as other Rab and Arf GTPases. FIPs have a highly conserved Rab11 binding domain and various conserved protein and phospholipid binding domains, differentially displayed by the various FIP proteins (schematized in Fig. 1A for FIP3) (24).

Although the role of Rab11 in membrane trafficking in several crucial cell physiological functions has been largely investigated, its role in receptor signal transduction remains poorly explored. The presence of the Src family tyrosine kinase Lck in Rab11 endosomes prompted us to investigate the role of Rab11 and its FIP effectors in TCR signal transduction leading to T cell activation and cytokine production. In this article, we show that FIP3 plays a key role in Lck transport and subcellular distribution. Its expression influences Lck targeting to the immunological synapse and early and late T cell activation events. Our work underscores the importance of Rab11-mediated endosomal traffic in regulating the spatial and temporal localization of TCR signaling molecules and, as a consequence, in the regulation of T cell activation.

Materials and Methods

Expression vectors, small interfering RNA, and Abs

Expression vectors. pEGFP-C3/FIP1, pEGFP-C1/FIP2, pEGFP-C1/FIP4, pEGFP-C1/FIP5, pEGFP-C1/FIP3 wild type (WT), and I738E mutant expression vectors have been previously described (25). pEGFPN1/Rab11, Q70L (constitutively active mutant), and S25N (dominant negative mutant) were provided by Dr. A. Echard (Institut Pasteur, Paris, France).

Small interfering RNA. FIP3 was depleted with small interfering RNA (siRNA) duplexes based on a human FIP3 sequence described elsewhere: siFIP3.1 (5′-AAGGGATCACAGCCATCAGAA-3′) (26) and siFIP3.2 (5′-AAGGCAGTGAGGCGGAGCTGTT-3′) (27). Lck silencing was accomplished using an siRNA oligonucleotide SMARTpool from Dharmacon.

Antibodies. The following Abs were used: For Western blot, rabbit anti-FIP3 (www.antibodies-online.com) was used at 2.4 μg/ml; mouse IgG1 anti-TCRζ (clone 6B10.2; Santa Cruz Biotechnology) was used at 0.2 μg/ml; mouse IgG2a anti–phospho-TCRζ, pY242 (clone K25-407.69; Becton Dickinson) was used at 0.05 μg/ml; rabbit IgG anti–phospho-ZAP70, pY319, rabbit anti–phospho-LAT, pY171, and rabbit anti–phospho-Lck, pY394 (Cell Signaling Technology) were used at 1/1000 dilution; and mouse IgG2b anti–β-tubulin (clone KMX-1; Millipore) was used at 0.2 μg/ml. For immunofluorescence, mouse monoclonal IgG2a anti-Rab11 (clone 102; Becton Dickinson) was used at 25 μg/ml; mouse IgG2b anti-Lck (clone 3A5; Santa Cruz Biotechnology) was used at 2 μg/ml; mouse IgG1 anti-CD3ε (clone UCHT1; BioLegend) was used at 10 μg/ml; mouse IgG1 anti-ZAP70 (1E7.2; Thermo clone) was used at 15 μg/ml; mouse IgG2b anti-Fyn (FYN-01; Abcam) was used at 10 μg/ml; and mouse IgG1 anti-Itk (clone 2F12; Becton Dickinson) was used at 5 μg/ml. For flow cytometry, mouse IgG1 anti-CD3ε (clone UCHT1; BioLegend) was used at 10 μg/ml. Cell stimulation was carried out with anti-CD3 (UCHT1) and anti-CD28 (clone CD28.2; Beckman Coulter) at the indicated concentrations.

Cell culture and transfection

Human peripheral blood T cells from healthy donors were obtained through the Institut Pasteur Clinical Investigation and Access to Biological Resources (ICAReB) core facility under protocols approved by the Committee of Protection of Persons, Ile de France-1 (2010-dec-12483) and from the French Blood Bank Organization (Etablissement Français du Sang). Informed consent was obtained from all subjects. $CD4^+$ T cells were isolated using the $CD4^+$ T Cell Isolation Kit II (Miltenyi Biotec) and cultured in RPMI 1640 medium containing 10% FCS, 1 mM sodium pyruvate, and nonessential amino acids. $CD4^+$ T cells were transfected with 1 nmol of siRNA using a Nucleofector system and the Human T Cell Nucleofector kit (Lonza). Cells were harvested and processed for analysis 72 h after transfection.

The human T cell line Jurkat clone J77cl20 and the APCs Raji were previously described (6). Jurkat were cultured in RPMI 1640 containing 10% FCS. For siRNA, two transfections of 10^7 Jurkat cells were performed at a 24-h interval using 1 nmol of control or FIP3 siRNA with a Neon Transfection system (Life Technologies), using the following protocol: 1400 V, 10 ms, three pulses. Cells were harvested and processed for analysis 72 h after the first transfection. For plasmid, 10 μg of DNA was electroporated into 10^7 Jurkat cells, using the Neon Transfection system, with the same protocol. Cells were harvested and processed for analysis 24 h after DNA transfection.

Confocal imaging

For immunological synapse formation, APCs (Raji) were pulsed with 10 μg/ml *Staphylococcus* enterotoxin E superantigen, then incubated 30 min at 37°C with transfected Jurkat cells in RPMI 1640 medium. Cells were plated onto poly-L-lysine–coated coverslips, using 0.002% (w/v) in water, molecular mass 150–300 kDa (Sigma-Aldrich). After 2 min, cells were fixed in PBS supplemented with 4% paraformaldehyde for 20 min at room temperature. After PBS wash, nonspecific binding was prevented by 15-min incubation, in PBS, 1% BSA (w/v) (PBS-BSA). Coverslips were then incubated 1 h at room temperature in PBS-BSA supplemented with 0.1% (v/v) Triton X-100 and the indicated primary Ab. Coverslips were then rinsed three times in PBS-BSA and incubated 1 h with the corresponding fluorescent-coupled secondary Ab. After three washes in PBS, coverslips were mounted on microscope slides, using 10 μl of ProLong Gold Antifade mounting medium with DAPI (Life Technologies). Confocal microscopy analyses were carried out in an LSM 700 confocal microscope (Carl Zeiss) equipped with a Plan-Apochromat ×63 objective.

The acquisition of images was done with ZEN (Carl Zeiss). Z-stack optical sections were acquired at 0.2-μm depth increments, and both green and red laser excitation were intercalated to minimize cross-talk between the acquired fluorescence channels.

Confocal image posttreatment

Complete image stack deconvolution was performed with Huygens Pro (version 14.10; Scientific Volume Imaging), and 2D images were generated from a sum intensity projection over a 3D volume cut of 0.4-μm depth, centered either on the vesicular compartment, when visible, or on a midsection of the cell. Colocalization analysis was performed by cropping the whole compartment (Rab11 or FIP3), or the whole cell, using Fiji software (28) with the Colocalization Threshold plugin. Threshold was automatically determined using the Costes method autothreshold determination (29). Pearson's correlation coefficient was calculated for the analysis. Statistical analyses were carried out by the nonparametrical Mann–Whitney *U* test using Prism software (GraphPad).

Images to quantify Lck accumulation at the immunological synapse were acquired at 1-μm increments in the *z*-axis to avoid fluorescence overlap. Fluorescence intensity at the synapse was calculated as percentage of the total fluorescence of the cell.

Protein phosphorylation analysis

Cells were stimulated by incubation with 10 μg/ml soluble anti-CD3 mAb (UCHT1) at 37°C. At the indicated time, ice-cold PBS was added to stop activation and cells were kept on ice until lysis. Cells were lysed for 30 min in ice-cold buffer composed of 20 mM Tris (pH 7.4), 0.25% lauryl-β-maltoside, 4 mM orthovanadate, 1 mM EGTA, 50 mM NaF, 10 mM $Na_4P_2O_7$, 1 mM $MgCl_2$, and protease inhibitors (1 mM AEBSF, 10 μg/ml aprotinin, 10 μg/ml leupeptin). Insoluble material was removed by centrifugation at 20,800 × *g* for 10 min at 4°C. Protein electrophoresis was performed on the lysate of 200,000 cells per time point, using NuPAGE 4–12% Bis-Tris gels (Life Technologies). After protein electrotransfer on nitrocellulose (LI-COR Biosciences), immunoblots were saturated with blocking buffer for near-infrared fluorescent Western blotting (Rockland Immunochemicals) and incubated with primary Abs. After incubation with secondary Abs Alexa Fluor 680 (Invitrogen) or DyLight 800 (Thermo Fisher Scientific), near-infrared fluorescence was detected by using an Odyssey scanner (LI-COR Biosciences) and quantified using National Institutes of Health ImageJ software.

Intracellular calcium analysis

A total of 3×10^6 cells were incubated in the dark with 40 μM Fluo-3-AM (Life Technologies) for 30 min at room temperature, washed once in RPMI 1640 medium containing 1% FCS, and resuspended in 2 ml of the same medium. Variations of free intracellular calcium concentration before and after activation with 10 μg/ml soluble anti-CD3 (UCHT1) were measured using a FACSCalibur flow cytometer (BD Biosciences) and analyzed using FlowJo v9 software (Tree Star). Incubating cells with 1 mM $MnCl_2$ or 2 μg/ml A-23187 allowed measuring minimum and maximum Fluo-3-AM signal, respectively, and normalization of the possible differences in Fluo-3 loading by the different cell lines analyzed. Intracellular calcium concentration was calculated using the formula previously described: $[Ca^{2+}]_i = K_d(F - F_{min})/(F_{max} - F)$, where K_d is 400 nM at vertebrate ionic strength as described previously (30).

Il-2 gene mRNA measurements by retrotranscription quantitative PCR

Jurkat or human peripheral blood CD4 T cells were activated for various times with anti-CD3 (UCHT1 at 500 ng/ml) and anti-CD28 (clone CD28.2 at 1 μg/ml). Total RNA was prepared by using the RNeasy Kit (Qiagen), according to the manufacturer's instructions; the step of on-column DNase I digestion was included to avoid potential DNA contamination. cDNA was generated from 500 ng of total RNA using iScript cDNA synthesis kit (Bio-Rad). In all cases, 2 μl of a 2.5 dilution of generated cDNA solution was used as a template for retrotranscription quantitative PCR (RT-qPCR). Gene products were quantified by RT-qPCR with the ABI PRISM 7900HT sequence detection system, using FastStart Universal SYBR Green PCR master mix (Roche). Each experiment was performed at least in triplicate, and RT-qPCR quantifications were performed in triplicates. RT-qPCR quantity values were calculated by the relative standard curve method. Values were normalized to the expression of *B2M* in Jurkat cells or *RPL13A* in primary T cells housekeeping genes. Primer sequences were as follows: IL-2, forward 5′-ACCTCAACTCCTGCCACAAT-3′, reverse 5′-TGAGCATCCTGGTGAGTTTG-3′; B2M, forward 5′-TGACTTTGTCACAGCCCAAGATA-3′, reverse 5′-AATGCGGCATCTTCAAACCT-3′; RPL13A, forward 5′-CATAGGAAGCTGGGAGCAAG-3′, reverse, 5′-GCCCTCCAATCAGTCTTCTG-3′.

Statistical analysis

Statistical analyses were carried out by the nonparametrical Mann–Whitney *U* test using Prism software (GraphPad V.6). The *p* values are represented as follows: $****p < 0.0001$, $***p < 0.001$, $**p < 0.01$, $*p < 0.05$, $p \geq 0.05$, nonsignificant.

Results

Rab11-FIP3 regulates Lck subcellular localization and intracellular traffic

In agreement with previous reports by us and others (12, 14), we observed Lck localized at the plasma membrane and in a $Rab11^+$ pericentrosomal compartment in both Jurkat and primary peripheral blood human CD4 T cells (Fig. 1B). Lck shuttles back and forth between the plasma membrane and the endosomal compartment and is targeted to the immunological synapse upon Ag recognition (7, 8, 13, 31). To investigate the importance of Rab11 regulation in Lck vesicle traffic, we analyzed the involvement of Rab11-FIP effectors. To this end, we individually expressed in Jurkat T cells GFP-tagged forms of each of the five members of the Rab11-FIP family (24) and analyzed their specific influence on Lck intracellular localization. Rab11-FIP3 and its close homolog FIP4 colocalized with Lck in the pericentrosomal compartment (Fig. 1C). Moreover, FIP3, and to a lesser extent FIP4, but not any of the other FIPs, induced the accumulation of Lck in this compartment, reducing Lck presence at the plasma membrane (Fig. 1C). Consistently, overexpression of FIP3 or FIP4, but not the other FIPs, inhibited Lck clustering at the immunological synapse (Fig. 1E). We therefore selected FIP3 for a deeper analysis. In contrast with Lck, the intracellular localization of other early TCR signaling protein tyrosine kinases, Fyn, ZAP70, and Itk, was not affected by FIP3 overexpression (Fig. 1D).

We observed that FIP3 overexpression induced the accumulation of Lck in a pericentrosomal compartment in which Lck strongly colocalized with FIP3 (Fig. 2A, 2B). In contrast, the FIP3-I738E point mutant, which does not bind to Rab11 (schematized in Fig. 1A) (32), did not colocalize with Lck. Its overexpression led to the opposite effect on Lck localization, preventing its association with the endosomes and localizing it preferentially at the plasma membrane (Fig. 2A, bottom panel, 2C). Moreover, two siRNA oligonucleotides directed to different sequences effectively reduced FIP3 expression (Fig. 2D) and prevented Lck pericentrosomal localization, dispersing it in small vesicles all over the cytoplasm and significantly inhibiting Rab11-Lck colocalization (Fig. 2E, 2F). We used FIP3.1 siRNA for the rest of the study because it induced less cell toxicity. To further investigate the role of Rab11 in Lck vesicle traffic, we overexpressed WT, constitutively active, and dominant negative Rab11 proteins. Consistent with FIP3 effects, overexpression of WT or constitutively active (GTP-bound, Q70L) increased the concentration of Lck in the Rab11 pericentrosomal compartment, where they colocalized with Lck (Fig. 2G, top and middle panels, 2H). Conversely, the dominant negative mutant (GDP-bound, S25N) induced Lck dispersion throughout the cytoplasm and did not colocalize with Lck (Fig. 2G, bottom panels, 2H).

These data show that Lck is associated with Rab11 endosomes, and its traffic and subcellular localization depend on the Rab11 effector FIP3.

FIP3 silencing inhibits TCR signal transduction

Lck is critical for TCR signal transduction (33), but how subcellular localization of Lck and its intracellular vesicle traffic contribute to regulate TCR signaling is ill defined. The potential role of Lck intracellular vesicle traffic was suggested in previous work by us and others showing that the accumulation of Lck in recycling

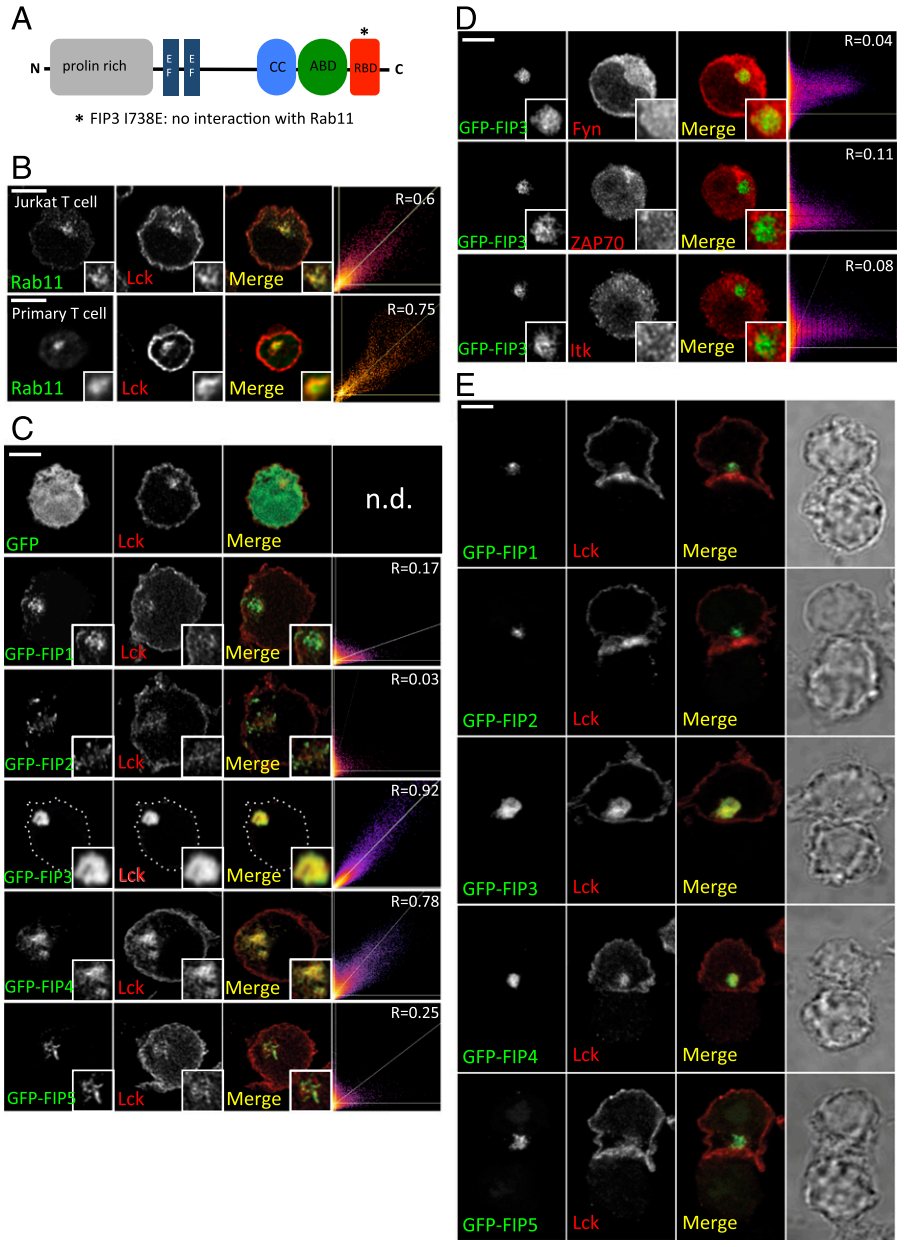

FIGURE 1. Effect of Rab11-FIPs on the subcellular localization of Lck. (**A**) Schematic representation of FIP3 structural features: proline-rich region, EF-hand domain, coiled-coil domain (CC), Arf binding domain (ABD), and Rab binding domain (RBD). Asterisk (*) represents the I738E point mutation that prevents Rab11 binding to FIPs (24). (**B**) Intracellular localization of Lck and Rab11 in Jurkat (top panels) and primary CD4 T cells from healthy donors (bottom panels) assessed by immunofluorescence. (**C**) Jurkat cells were transfected with expression vectors encoding GFP, GFP-FIP1, GFP-FIP2, GFP-FIP3, GFP-FIP4, or GFP-FIP5. Endogenous Lck was detected by immunofluorescence. (**D**) Cells were transfected with GFP-FIP3, and endogenous Fyn, ZAP70, and Itk were detected by immunofluorescence. (**E**) Cells were transfected as in (C) and allowed to form immunological synapses with superantigen-pulsed Raji cells for 30 min. Endogenous Lck was detected by immunofluorescence and confocal microscopy. (B–E) Cells were analyzed by confocal microscopy acquiring a Z-stack of confocal optical sections at 0.2-μm steps. 3D confocal images were posttreated by deconvolution. A 0.4-μm-thick medial stack is shown. The pericentrosomal vesicular compartment is magnified at the bottom right-hand corner of each image. Scale bars, 5 μm. Colocalization in the pericentrosomal compartment of endogenous Lck and Rab11, or Lck and each GFP-FIP was assessed by the Pearson's correlation coefficient (R), as described in *Materials and Methods.* Visual microscopy analyses of 100–150 cells per transfection in two different experiments were performed to determine the localization of Lck with respect to Rab11, the effect of overexpressing the different FIPs on Lck intracellular localization, in resting cells, or in cells forming immunological synapses, and the effect of FIP3 overexpression on Fyn, ZAP70, and Itk tyrosine kinase subcellular localization. The representative phenotype of each FIP overexpression and Pearson's correlation coefficient is shown.

endosomes caused by HIV-1 infection, or by depletion of the transport protein MAL or the Unc119 protein, impaired immunological synapse formation and inhibited TCR signaling (8, 13, 14). Moreover, Nika et al. (34) reported that Lck activity did not vary upon TCR stimulation, suggesting that Lck capacity to phosphorylate its substrates might result from controlled changes of its subcellular localization.

To directly address the regulatory role of Lck localization and transport on TCR signaling, we analyzed the consequences of altering Rab11-mediated Lck vesicle traffic by means of FIP3 siRNA silencing. We observed that Lck-dependent early TCR signaling events, like the tyrosine phosphorylation of TCRζ, ZAP70, and LAT, and increase in intracellular calcium concentration upon anti-CD3 stimulation were inhibited in FIP3-silenced

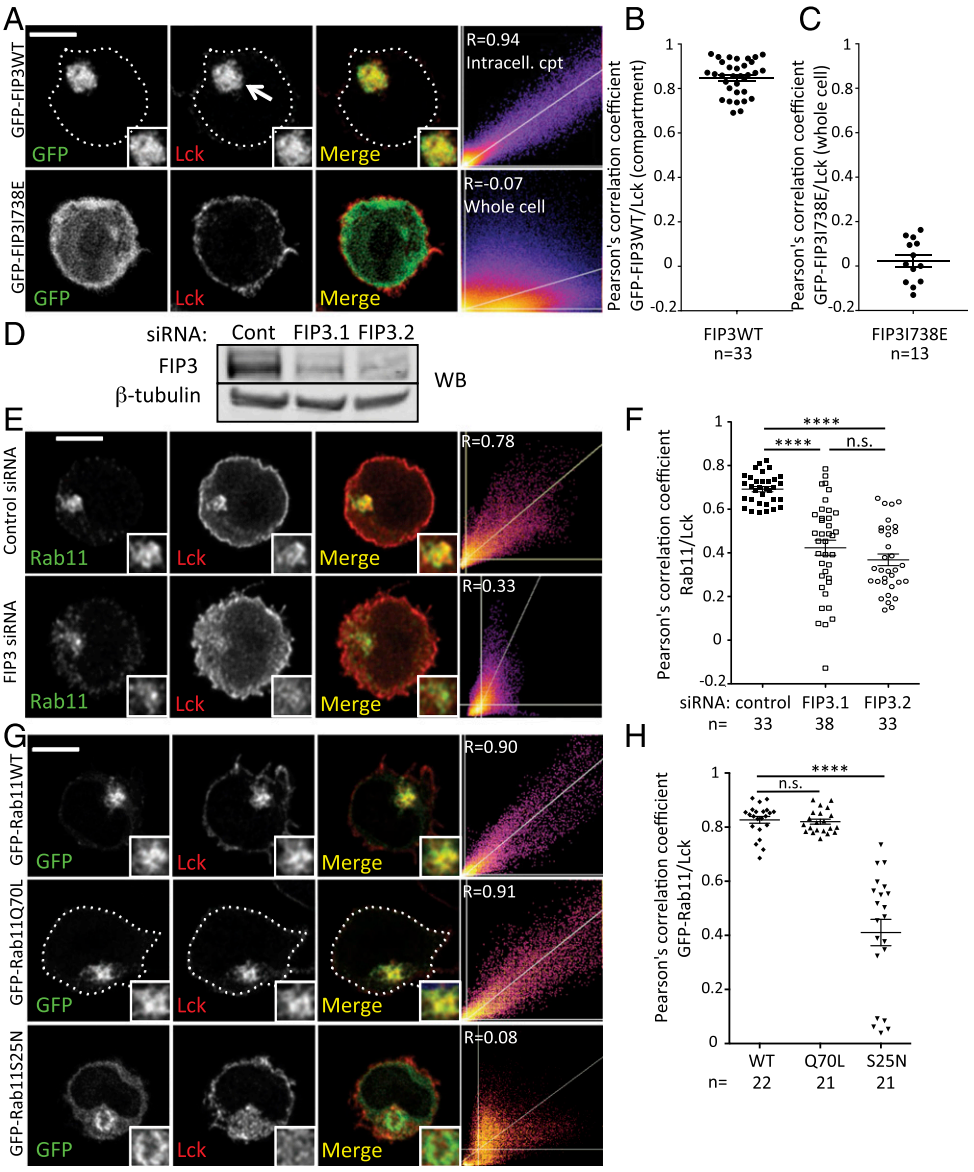

FIGURE 2. Lck endosomal localization is regulated by Rab11-FIP3. (**A**) Jurkat cells were transfected with expression vectors encoding GFP-FIP3-WT or GFP-FIP3-I^{738}E. Endogenous Lck was detected by immunofluorescence. (**B** and **C**) Colocalization between endogenous Lck and GFP-FIP3-WT in the pericentrosomal compartment, or between Lck and the GFP-FIP3-I^{738}E mutant in the whole cell was assessed by Pearson's correlation coefficient (R) as described in *Materials and Methods*. Each dot represents one cell. (**D**) Jurkat T cells were transfected with control, FIP3.1, or FIP3.2 siRNA oligonucleotides, and FIP3 expression was analyzed by Western blot, with respect to β-tubulin expression. (**E**) Jurkat T cells were treated with control or siFIP3.1 siRNA, and intracellular distribution of endogenous Rab11 and Lck was assessed by immunofluorescence and confocal microscopy. (**F**) Colocalization between Lck and Rab11 was determined by Pearson's correlation coefficient (R) as in (B). (**G**) Jurkat cells were transfected with expression vectors encoding Rab11-WT-GFP, Rab11-Q^{70}L-GFP (constitutively active mutant), or Rab11-S^{25}N-GFP (dominant negative mutant). Endogenous Lck was detected by immunofluorescence. (**H**) Colocalization between endogenous Lck and GFP-Rab11-WT, GFP-Rab11Q70L, or GFP-Rab11-S25N in the pericentrosomal compartment was determined by Pearson's correlation coefficient (R) as in (B) and (F). (A, E, and G) A Z-stack of confocal optical sections at 0.2-μm steps was acquired. 3D confocal images were posttreated by deconvolution. A 0.4-μm-thick medial stack is shown. The pericentrosomal vesicular compartment is magnified at the bottom right-hand corner of each image. Images are representative of three experiments. Scale bars, 5 μm. (B, C, F, and H) Pearson's correlation (R) population analysis; each dot represents one cell. Horizontal bars represent the mean ± SEM, Mann–Whitney *U* test. $^{****}p < 0.0001$, $^{n.s.}p \geq 0.05$.

cells (Fig. 3A–C). Interestingly, basal phosphorylation of these proteins in nonstimulated cells, as well as the intracellular calcium concentration, were lower in FIP3-silenced cells (Fig. 3A–C, time 0). These effects were unlikely due to the reduction of Lck kinase activity, because the rate of phosphorylation of Tyr^{394}, which controls Lck kinase activity, remained unchanged in control and FIP3-silenced cells upon CD3 stimulation (Fig. 4A, 4B). Moreover, we observed that Tyr^{394}-phosphorylated Lck followed similar localization patterns to total Lck. Thus, Tyr^{394}-phosphorylated Lck was localized at the plasma membrane, as well as in pericentrosomal endosomes in control siRNA–treated cells, and it was associated with small vesicle–type structures located all over the cytoplasm in FIP3-silenced cells (Fig. 4C).

TCR stimulation leads to the activation of cytokine genes, like IL-2. We therefore investigated the effect of FIP3 silencing in IL-2 mRNA levels upon T cell activation with anti-CD3 + anti-CD28 Abs, as assessed by RT-qPCR. Consistent with the inhibition of early TCR signaling events, IL-2 mRNA levels observed after 2 h

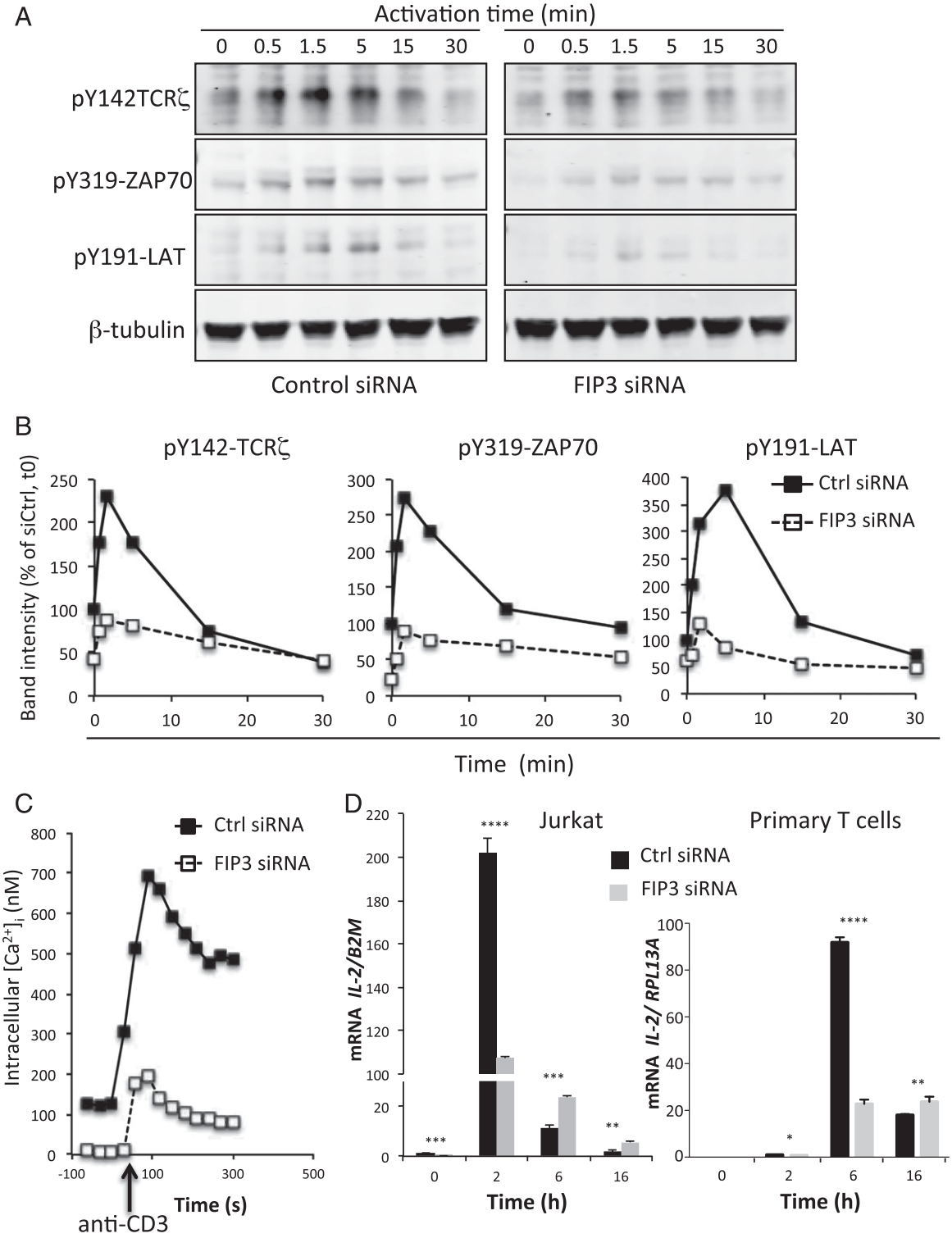

FIGURE 3. Rab11-FIP3 silencing impairs T cell activation events. (**A**–**C**) Jurkat T cells transfected with control or FIP3.1 siRNA oligonucleotides were activated with anti-CD3 (UCHT1) for the indicated time. (A) Phosphorylation of TCRζ, ZAP70, and LAT was analyzed by Western blot with the depicted specific anti-phosphotyrosine Abs. (B) Graphs represent the percentage of each band intensity with respect to that of nonstimulated cells ($t = 0$) transfected with control siRNA. The intensity of each band from Western blots shown in (A) was normalized with respect to the intensity of β-tubulin for each time point. (C) Intracellular calcium concentration was measured by loading Jurkat cells with FLUO-3 AM calcium indicator. Intracellular calcium concentration was measured by flow cytometry. (**D**) Jurkat (left panel) or peripheral blood CD4 T cells (right panel) were transfected as in (A)–(C). Cells were activated with anti-CD3 + anti-CD28 Abs. *IL2* mRNA levels were assessed by RT-qPCR and normalized to the *B2M* (Jurkat) or *RPL13A* (primary T cells) housekeeping genes mRNA. Data are the mean of $n = 3$ RT-qPCRs representative of three independent biological experiments (four different donors for primary T cells). Mean ± SD. Mann–Whitney *U* test. $^{****}p < 0.0001$, $^{***}p < 0.001$, $^{**}p < 0.01$, $^{*}p < 0.05$.

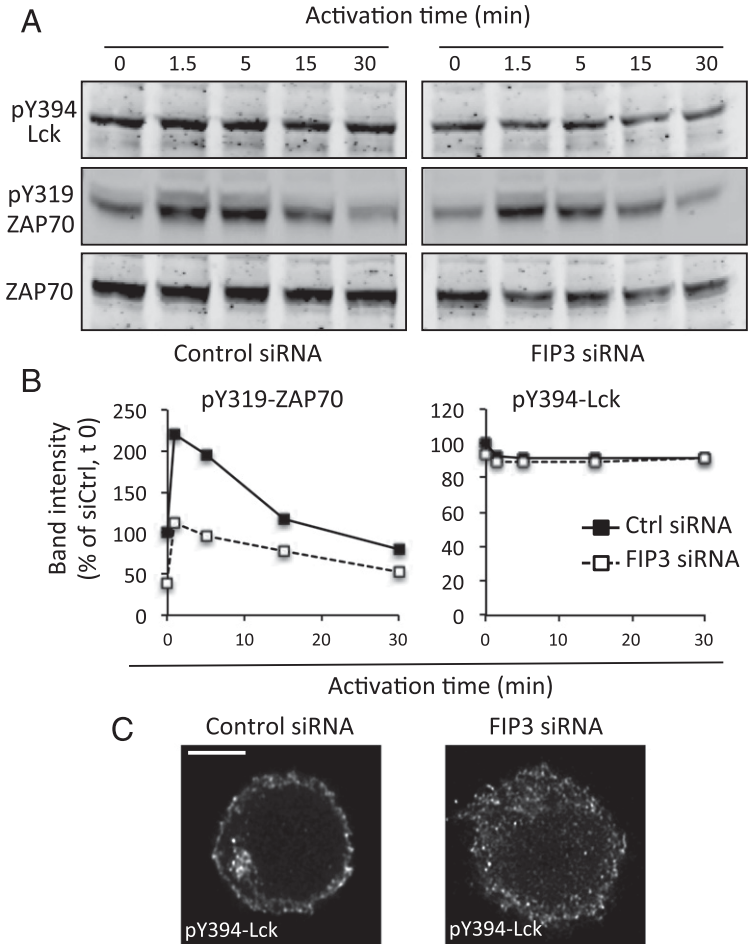

FIGURE 4. Rab11-FIP3 controls TCR signaling downstream of Lck. (**A**) Jurkat T cells transfected with control or FIP3.1 siRNA oligonucleotides were activated with anti-CD3 (UCHT1) for the indicated time. Phosphorylation of Lck and ZAP70 was analyzed by Western blot with the depicted specific anti-phosphotyrosine Abs. (**B**) Graphs represent the percentage of intensity of each band with respect to that of nonstimulated cells (t = 0) transfected with control siRNA. The intensity of each band from Western blots shown in (A) was normalized with respect to the intensity of ZAP70 for each time point. (**C**) Intracellular localization of Lck-pY394 in control or FIP3 siRNA-transfected, nonstimulated Jurkat cells. Endogenous Lck was detected by immunofluorescence and confocal microscopy. 3D confocal images were posttreated by deconvolution. A 0.4-μm-thick medial stack is shown. Scale bar, 5 μm. Representative of three experiments.

of TCR/CD28 stimulation were significantly lower in FIP3-silenced Jurkat cells. Interestingly, at later time points of activation (6 and 16 h), the relative effect was inversed and FIP3-silenced cells displayed significantly higher levels of IL-2 mRNA than control cells. Similar results were obtained on primary CD4 T cells from healthy donors, although the kinetics was delayed with respect to Jurkat cells (Fig. 3D, right panel).

Altogether, these findings indicate that Lck subcellular localization controlled by Rab11-FIP3–mediated intracellular traffic regulates T cell activation at steady-state, as well as in response to TCR engagement that ultimately leads to IL-2 gene expression.

Rab11-FIP3 controls Lck translocation to the immunological synapse

Because Lck targeting to the immunological synapse depends on its intracellular vesicle traffic (8, 12–14), we asked whether FIP3 plays a role in regulating this event. Overexpression of FIP3-WT, which induces Lck accumulation in the Rab11 pericentrosomal compartment, significantly inhibited Lck clustering at the immunological synapse between T cells and superantigen-loaded APCs (Fig. 5A, middle panel, 5C). Surprisingly, although the overexpression of the Rab11 binding–deficient FIP3-IE mutant delocalized most of the Lck from the intracellular compartment to the plasma membrane, it also prevented Lck accumulation at the synapse (Fig. 5A, bottom panel, 5C). Moreover, despite their effects on steady-state subcellular localization of Lck, overexpression of wild-type, constitutively active, or dominant negative Rab11 mutants caused no significant changes on the pattern of Lck accumulation at the synapse, or Lck accumulation in that area (Fig. 5B, 5C). Finally, in contrast with FIP3-WT or FIP3-IE mutant overexpression, FIP3 silencing by siRNA did not significantly alter the percentage of Lck localized at the T cell APC contact (Fig. 5D, 5E). However, T cell–APC contact sites appeared significantly larger and dissymmetric, as we have recently described (35), displaying a more dispersed localization of Lck and TCR clusters at the immunological synapse. Finally, the dispersion of values in siFIP3-treated cells was greater, suggesting that a mild effect on Lck localization was occurring in FIP3-silenced cells (Fig. 5D, bottom panels, 5E).

Altogether, these data show that Lck traffics through the Rab11 ERC and its intracellular transport is regulated by Rab11-FIP3 interactions. Importantly, Lck endosomal traffic is necessary for its regular clustering at the immunological synapse, because constraining Lck localization to the pericentrosomal compartment or to the plasma membrane inhibited Lck accumulation at the synapse.

Rab11-FIP3 silencing upregulates TCR-CD3 surface expression by increasing TCRζ levels

We have shown previously that the TCR-CD3 complex traffics through the transferrin receptor–positive endosomal pathway, being continuously internalized and recycled back to the plasma membrane, and translocated to the immunological synapse via endosomal transport (6). Because the transferrin receptor–positive intracellular pathway overlaps with the Rab11$^+$ recycling endosomal compartment (36), FIP3 silencing could affect TCR-CD3 trafficking and, as a consequence, TCR-CD3 cell surface expression and its capacity to transduce activation signals. Therefore, we investigated whether FIP3 silencing was affecting the amount of TCR-CD3 at the cell surface and/or its endocytosis-recycling equilibrium. Interestingly, the level of surface TCR-CD3 was

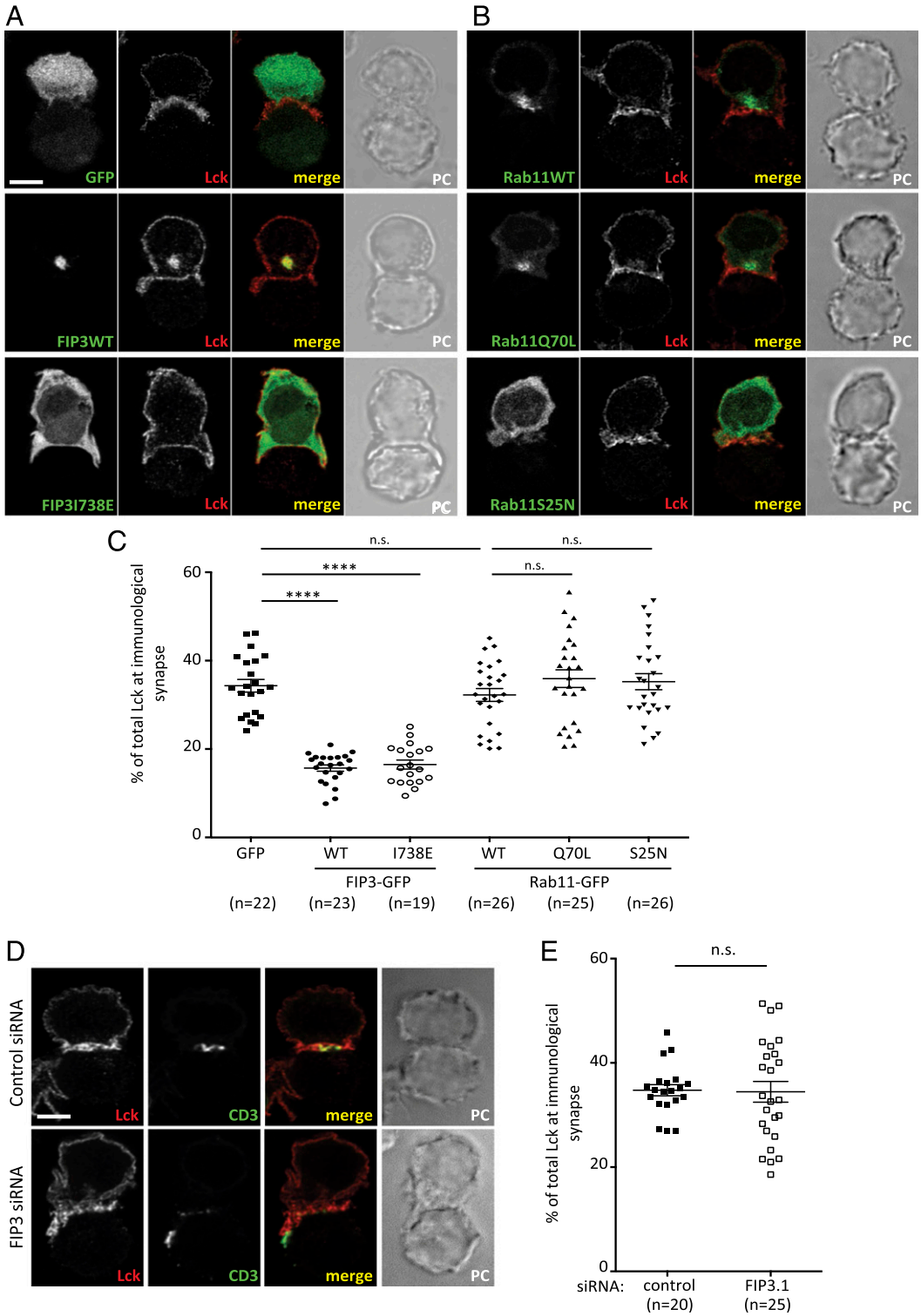

FIGURE 5. Rab11-FIP3 controls Lck clustering at the immunological synapse. (**A**–**C**) Jurkat T cells were transfected with expression vectors encoding GFP, GFP-FIP3-WT, GFP-FIP3I^{738}E, GFP-Rab11-WT, GFP-Rab11Q^{70}L (constitutively active), or GFP-Rab11S^{25}N (dominant negative). (**D** and **E**) Jurkat cells were transfected with control or FIP3.1 siRNA. Cells were allowed to form immunological synapses with *Staphylococcus* enterotoxin E superantigen–pulsed Raji cells for 30 min. Intracellular distribution of surface CD3 and/or endogenous Lck was detected by immunofluorescence and confocal microscopy. A Z-stack of confocal optical sections was acquired at 0.2-μm steps. 3D confocal images were posttreated by deconvolution. A 0.4-μm-thick medial stack is shown. Images are representative of three experiments. (C and E) Amount of Lck at the immunological synapse relative to the total cellular Lck. Each dot represents one cell. Horizontal bars represent the mean ± SEM, Mann–Whitney *U* test. Scale bars, 5 μm (A, D). ****$p < 0.0001$, $^{n.s.}p \geq 0.05$.

significantly augmented (≈2-fold) in both FIP3-silenced Jurkat and primary CD4 T cells, whose Lck compartment was also disrupted (Fig. 6A, 6E, 6F). Nonetheless, no significant increase in the amount of total CD3 was observed, as assessed by immunofluorescence staining and FACS analyses in permeabilized cells (Fig. 6B). The endocytic and recycling traffic of TCR-CD3 seemed not to be affected by FIP3 silencing, as assessed by the capacity of the TCR-CD3 complex to be internalized and recycled

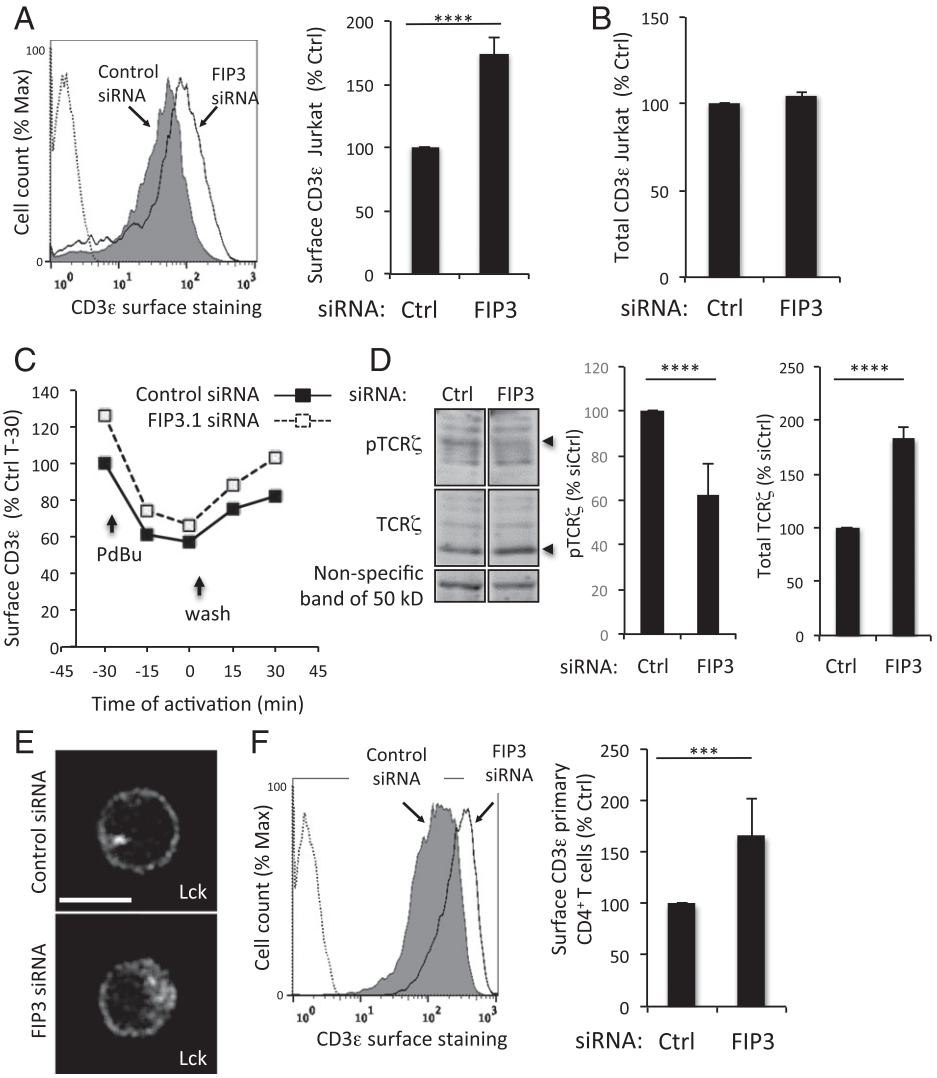

FIGURE 6. Rab11-FIP3 silencing increases TCR-CD3 cell surface expression. (**A**–**D**) Jurkat T cells were transfected with control or FIP3.1 siRNA. (A) Cell surface and (B) total CD3ε were measured by flow cytometry on nonpermeabilized (A) or permeabilized cells (B), respectively. Results are expressed as the percentage of fluorescence intensity with respect to cells transfected with control siRNA. (A, left panel) Representative of six experiments. (A, right panel, and B) Mean ± SD of six experiments, Mann–Whitney *U* test. (C) Jurkat cells were incubated with the phorbol ester PDBu (1 μM) for 30 min at 37°C. Cells were then washed at 4°C ($t = 0$) to remove PDBu and incubated again for the indicated times at 37°C. At each time point, CD3 surface expression was analyzed by flow cytometry. Results are expressed as percentage of CD3 expressed at the cell surface at each time of PDBu incubation, with respect to untreated control siRNA-transfected cells at $t = 0$. Representative of two experiments. (D) Phosphorylation of TCRζ at Y142 and total TCRζ were assessed in Jurkat cells by Western blot and normalized with respect to a nonspecific band of 50 kDa. The percentage of pTCRζ or TCRζ in cells transfected with siFIP3 was then calculated with respect to cells transfected with control siRNA. Mean ± SD of three experiments, Mann–Whitney *U* test. (**E** and **F**) Primary CD4 T cells from healthy donors were transfected with control or FIP3.1 siRNA. (E) Endogenous Lck was localized by immunofluorescence and confocal microscopy. 3D confocal images were posttreated by deconvolution. A 0.4-μm-thick medial stack is shown. Scale bar, 5 μm. (F) Cell surface CD3 was measured by flow cytometry in nonpermeabilized cells. Results are expressed as the percentage of fluorescence intensity with respect to cells transfected with control siRNA. Mean ± SD of three experiments, Mann–Whitney *U* test. ****$p < 0.0001$, ***$p < 0.001$.

back to the cell surface upon incubation with, and washing of, phorbol 12,13-dibutyrate (PDBu) (6, 8) (Fig. 6C).

The expression of the TCRζ subunit was shown to stabilize the TCR-CD3 complex at the plasma membrane, modulating TCR-CD3 cell surface expression (37). Moreover, TCRζ degradation rate is controlled by Lck, and TCRζ phosphorylation was pinpointed as a signal for TCRζ degradation in lysosomes (38). Therefore, we investigated whether perturbation of Lck subcellular localization by FIP3-silencing, which results in lower TCRζ phosphorylation (Fig. 3A, 3B), could modify the steady-state amount of TCRζ. FIP3 silencing indeed led to a significant increase in TCRζ total level, concomitant with a decrease in TCRζ tyrosine phosphorylation (Fig. 6D). In line with these findings, Lck silencing had a similar effect on TCR-CD3 surface expression as FIP3 silencing, and the double knockdown (FIP3 + Lck) did not have a significant cumulative effect (Fig. 7).

Altogether, these data indicate that FIP3 silencing leads to increased TCR-CD3 cell surface expression by reducing Lck-dependent TCRζ degradation and subsequently increasing TCRζ cellular levels. Mislocalization of Lck may prevent Lck-TCRζ encounters and, as a consequence, TCRζ tyrosine phosphorylation.

Discussion

Rab11-mediated endosomal recycling is central for the regulation of cell membrane dynamics (21, 22). We describe in this article a new role for this compartment. Our findings underscore the

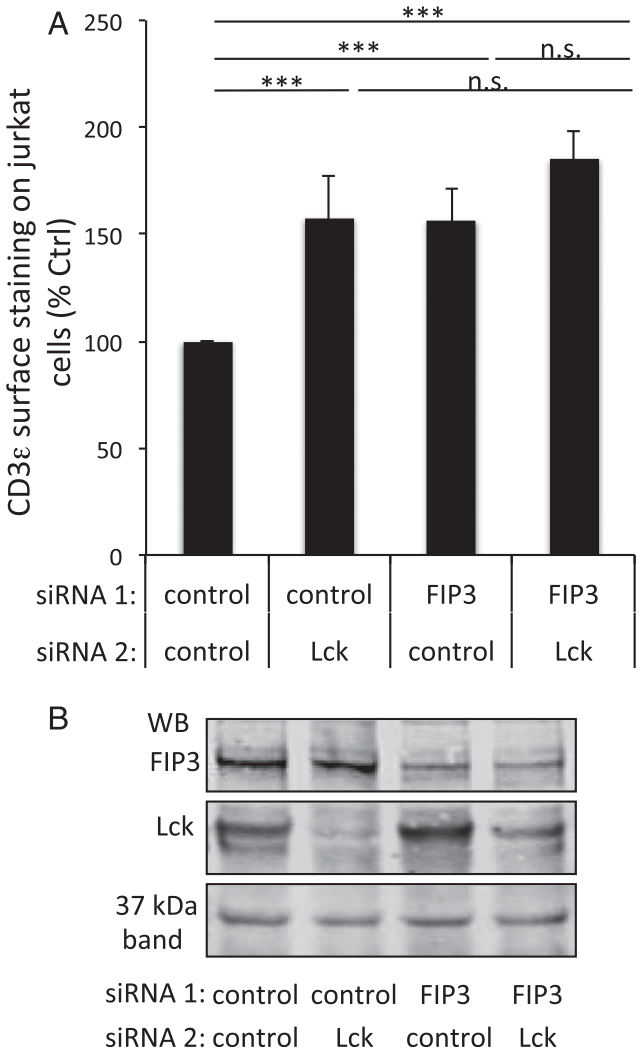

FIGURE 7. Rab11-FIP3 silencing upregulates TCR-CD3 cell surface expression in an Lck-dependent manner. (**A**) Jurkat T cells were transfected with two-by-two combinations of control, Lck, and FIP3.1 siRNA oligonucleotides. CD3 cell surface expression was then assessed by flow cytometry. Measurements are expressed as percentage of staining of cells transfected with control siRNA. Mean of triplicates ± SD, Mann–Whitney *U* test. Representative of three experiments. (**B**) FIP3 protein expression was analyzed by Western blot with respect to a nonspecific band of 37 kDa, used here as a loading control. $^{***}p < 0.001$, $^{n.s.}p \geq 0.05$.

importance of the Rab11 ERC and of the Rab11 effector FIP3 in regulating the capacity of T cells to transduce TCR activation signals leading to cytokine gene expression. Interestingly, several TCR signaling molecules, like Lck, TCRζ, and LAT, are associated with distinct endosomal vesicular compartments, but solely Lck was found to be associated with Rab11 endosomes (12) (detailed in the *Introduction*). Differential endosomal association may help to control steady-state encounters of critical signaling molecules within nonstimulated T cells, setting their basal phosphorylation level. Further on, concomitant polarized traffic of multiple endosomal compartments to the APC contact site upon local TCR stimulation by peptide-MHC may expedite localized encounters of the various signaling molecules at the immunological synapse, the formation of signaling complexes, and sustained TCR signaling.

Lck is the first tyrosine kinase recruited upon TCR engagement and is critical for TCR signal transduction (33). Rab11-mediated regulation of Lck traffic might therefore be key to initiate TCR signal transduction. This prompted us to screen the effect of FIPs, known to regulate Rab11 endosomal traffic in other cell types, on Lck intracellular traffic and function. Overexpression experiments showed that among the five FIP family members, only FIP3 and, to a lesser extent, its close homolog FIP4 modified Lck subcellular localization, accumulating Lck in the Rab11 pericentrosomal compartment. This effect was due to Rab11, because overexpression of the FIP3-I738E mutant, which does not bind to Rab11, induced the opposite effect, driving Lck localization mostly to the plasma membrane.

Unbalancing Lck accumulation toward pericentrosomal endosomes or toward the plasma membrane prevented Lck clustering at the synapse. This finding highlights the importance of endosomal-mediated traffic for Lck delivery to the immunological synapse. Interestingly, FIP3 silencing strongly perturbed steady-state Lck subcellular distribution and its colocalization with Rab11, but did not prevent Lck translocation to the T cell–APC contact zone. However, Lck distribution at the synapse appeared more fragmented and asymmetrically distributed. Synapse asymmetry is likely due to the additional effect of Rab11-FIP3 on the subcellular localization of Rac1 that we recently unveiled, and regulates actin remodeling and immunological synapse architecture (35). Importantly, FIP3 silencing has severe consequences for TCR signal transduction, because it inhibited tyrosine phosphorylation of TCRζ, ZAP70, and LAT and significantly reduced the increase of intracellular calcium concentration in response to TCR stimulation. It is worth noting that the basal levels of tyrosine phosphorylation of these proteins in nonstimulated cells were also significantly reduced, as well as the steady-state intracellular calcium concentration. Therefore, Lck endosomal traffic regulated by Rab11-FIP3 (32) orchestrates TCR-proximal signal transduction, maintaining steady-state levels of signaling in nonstimulated cells and helping to reach enhanced levels upon TCR triggering. This mechanism may control T cell responsiveness by setting the optimal level of Lck and TCR-CD3 levels at the plasma membrane. Of note, FIP3 silencing appears not to affect Lck activity, as judged by the unchanged level of phosphorylation of the Lck-activating residue Y394. Finally, the effects on signaling reported in this article were unlikely due to the subversion of intracellular traffic of other TCR-proximal protein tyrosine kinases. Indeed, the localization of Fyn, ZAP70, and Itk, which regulate, together with Lck, tyrosine phosphorylation and intracellular calcium, was not affected by FIP3 overexpression. Moreover, these kinases were not localized at the Rab11 endosomal compartment. Therefore, Lck needs to be associated with the correct vesicles and delivered to the appropriate subcellular localization to phosphorylate its substrates and to control TCR signaling.

Our findings raise the question whether TCR signal transduction may regulate FIP3–Rab11 interaction. This could occur by regulating Rab11 GDP-GTP exchange. Because FIP3 forms a tripartite complex with Rab11GTP and dynein (32), modulating Rab11GTP amounts could regulate Rab11 vesicle traffic and Lck localization. However, to our knowledge, it has not been reported that TCR-mediated signaling activates Rab11 GDP-to-GTP exchange. Our data show that overexpression of the Rab11GTP versus Rab11GDP mutants modifies to a certain extent the presence of Lck in the pericentrosomal compartment. However, it does not alter Lck clustering at the immunological synapse. This suggests that Rab11-FIP3 influences Lck traffic to the synapse through its interaction with dynein and microtubules. A subtle effect of Rab11 GDP-GTP exchange induced by TCR engagement cannot be ruled out, however.

We observed that FIP3 silencing resulted in increased TCR-CD3 cell surface expression, without apparently affecting TCR-CD3 endocytic and recycling traffic, or CD3 total levels. This is likely

the consequence of the inability of Lck to phosphorylate TCRζ and regulate its degradation, which in turn controls TCRζ steady-state levels (38) and finely regulates TCR-CD3 cell surface expression (37).

FIP3 regulation of Lck endosomal traffic is complementary of that exerted by the proteins MAL and Unc119, whose deficiency induces Lck retention in the pericentrosomal compartment and prevents Lck access to the plasma membrane. These proteins may contribute to the outward endosomal Lck traffic, from the centrosomal compartment to the plasma membrane (13, 14, 31). Conversely, FIP3 contributes to transport Lck, to the pericentrosomal compartment, and is necessary to keep Lck associated with Rab11 endosomes, because FIP3 overexpression concentrates Lck in the centrosomal compartment and FIP3 silencing strongly reduces Rab11-Lck colocalization. FIP3 could accomplish this function through its capacity to link Rab11 vesicles with dynein (32), a microtubule-based molecular motor that transports vesicles from the plus to the minus microtubule ends and is necessary to concentrate Rab11 recycling endosomes in the pericentrosomal region (32). Therefore, a finely regulated Lck endosomal traffic balancing inward and outward transport by means of different Rab11 effectors and traffic regulators is key to ensure the regulation of TCR signaling. Interestingly, HIV-1, through its protein Nef, subverts Lck endosomal traffic, retaining Lck in the pericentrosomal Rab11 compartment, preventing Lck clustering at the immunological synapse, and inhibiting TCR signaling. In this way, HIV-1 modulates the capacity of infected T cells to respond to antigenic stimulations (8).

An interesting observation is the relative effect of FIP3 silencing on IL-2 gene expression at earlier versus later activation times. Thus, although after 2 h of CD3 and CD28 stimulation IL-2 mRNA levels were significantly lower in FIP3-silenced cells, at later time points (6 and 16 h for Jurkat and 16 h for primary T cells), the opposite effect was observed, with IL-2 mRNA levels significantly higher in FIP3-silenced cells. IL-2 mRNA levels in both conditions were nevertheless lower than at early times. This apparent contradiction may be because of the differential balance of activation effects at earlier and later times. First, the inhibiting effect of FIP3 silencing on tyrosine phosphorylation of TCRζ, ZAP70, LAT, and calcium levels may dominate. Then, the fact of having more stable levels of TCR-CD3 at the cell surface might take over and maintain signaling for a longer time in FIP3-silenced cells. Additionally, FIP3 silencing may result in the activation of other signaling intermediates. For instance, we have observed FIP3 silencing also modifies Rac1 intracellular localization inducing cellular changes corresponding to Rac1 activation and increasing T cell spreading (35). Increased spreading on plate-bound anti-CD3, together with enhanced TCR-CD3 surface expression, may make TCR signal transduction more stable in the long term. Moreover, because Rac1 also activates Jun kinase and, as a consequence, the transcription factor AP-1 (Jun and Fos), it is possible that FIP3 activation could enhance downstream activation pathways leading to a more sustained IL-2 gene activation and cytokine production.

In conclusion, our study underlines the importance of Rab11-mediated intracellular traffic as a critical modulator of T cell signaling.

Acknowledgments

We thank Dr. A. Danckaert and the microscopy core facility Imagopole-Citech at the Institut Pasteur for continuous technical support. We thank Dr. A. Echard and Dr. S. Etienne-Manneville (Institut Pasteur), and Dr. O. Acuto, K. Nika, G. Massi, and A. L. Lanz (University of Oxford) for expression vectors reagents and cell lines, and Dr. A. Graziani (Universita Vita-Salute San Rafaele, Milan, Italy) for stimulating discussions. Blood samples from healthy donors were obtained from the French Blood Bank (Etablissement Français du Sang) and from the ICAReB core facility, in the framework of institutional research and clinical investigation projects approved by the Ethical Committees. The collaboration of Dr. M. N. Ungeheuer and Dr. I. Najjar (ICAReB) is thankfully acknowledged.

Disclosures

The authors have no financial conflicts of interest.

References

1. Acuto, O., V. Di Bartolo, and F. Michel. 2008. Tailoring T-cell receptor signals by proximal negative feedback mechanisms. *Nat. Rev. Immunol.* 8: 699–712.
2. Agüera-Gonzalez, S., J. Bouchet, and A. Alcover. 2015. Immunological synapse. In *eLS*. John Wiley & Sons, Ltd, Chichester, United Kingdom, p. 1–9.
3. Soares, H., R. Lasserre, and A. Alcover. 2013. Orchestrating cytoskeleton and intracellular vesicle traffic to build functional immunological synapses. *Immunol. Rev.* 256: 118–132.
4. Wülfing, C., and M. M. Davis. 1998. A receptor/cytoskeletal movement triggered by costimulation during T cell activation. *Science* 282: 2266–2269.
5. Blanchard, N., V. Di Bartolo, and C. Hivroz. 2002. In the immune synapse, ZAP-70 controls T cell polarization and recruitment of signaling proteins but not formation of the synaptic pattern. *Immunity* 17: 389–399.
6. Das, V., B. Nal, A. Dujeancourt, M. I. Thoulouze, T. Galli, P. Roux, A. Dautry-Varsat, and A. Alcover. 2004. Activation-induced polarized recycling targets T cell antigen receptors to the immunological synapse; involvement of SNARE complexes. *Immunity* 20: 577–588.
7. Ehrlich, L. I. R., P. J. R. Ebert, M. F. Krummel, A. Weiss, and M. M. Davis. 2002. Dynamics of p56lck translocation to the T cell immunological synapse following agonist and antagonist stimulation. *Immunity* 17: 809–822.
8. Thoulouze, M. I., N. Sol-Foulon, F. Blanchet, A. Dautry-Varsat, O. Schwartz, and A. Alcover. 2006. Human immunodeficiency virus type-1 infection impairs the formation of the immunological synapse. *Immunity* 24: 547–561.
9. Bonello, G., N. Blanchard, M. C. Montoya, E. Aguado, C. Langlet, H. T. He, S. Nunez-Cruz, M. Malissen, F. Sanchez-Madrid, D. Olive, et al. 2004. Dynamic recruitment of the adaptor protein LAT: LAT exists in two distinct intracellular pools and controls its own recruitment. *J. Cell Sci.* 117: 1009–1016.
10. Purbhoo, M. A., H. Liu, S. Oddos, D. M. Owen, M. A. Neil, S. V. Pageon, P. M. French, C. E. Rudd, and D. M. Davis. 2010. Dynamics of subsynaptic vesicles and surface microclusters at the immunological synapse. *Sci. Signal.* 3: ra36.
11. Larghi, P., D. J. Williamson, J. M. Carpier, S. Dogniaux, K. Chemin, A. Bohineust, L. Danglot, K. Gaus, T. Galli, and C. Hivroz. 2013. VAMP7 controls T cell activation by regulating the recruitment and phosphorylation of vesicular Lat at TCR-activation sites. *Nat. Immunol.* 14: 723–731.
12. Soares, H., R. Henriques, M. Sachse, L. Ventimiglia, M. A. Alonso, C. Zimmer, M. I. Thoulouze, and A. Alcover. 2013. Regulated vesicle fusion generates signaling nanoterritories that control T cell activation at the immunological synapse. *J. Exp. Med.* 210: 2415–2433.
13. Antón, O., A. Batista, J. Millán, L. Andrés-Delgado, R. Puertollano, I. Correas, and M. A. Alonso. 2008. An essential role for the MAL protein in targeting Lck to the plasma membrane of human T lymphocytes. *J. Exp. Med.* 205: 3201–3213.
14. Gorska, M. M., Q. Liang, Z. Karim, and R. Alam. 2009. Uncoordinated 119 protein controls trafficking of Lck via the Rab11 endosome and is critical for immunological synapse formation. *J. Immunol.* 183: 1675–1684.
15. Patino-Lopez, G., X. Dong, K. Ben-Aissa, K. M. Bernot, T. Itoh, M. Fukuda, M. J. Kruhlak, L. E. Samelson, and S. Shaw. 2008. Rab35 and its GAP EPI64C in T cells regulate receptor recycling and immunological synapse formation. *J. Biol. Chem.* 283: 18323–18330.
16. Finetti, F., S. R. Paccani, M. G. Riparbelli, E. Giacomello, G. Perinetti, G. J. Pazour, J. L. Rosenbaum, and C. T. Baldari. 2009. Intraflagellar transport is required for polarized recycling of the TCR/CD3 complex to the immune synapse. *Nat. Cell Biol.* 11: 1332–1339.
17. Finetti, F., L. Patrussi, D. Galgano, C. Cassioli, G. Perinetti, G. J. Pazour, and C. T. Baldari. 2015. The small GTPase Rab8 interacts with VAMP-3 to regulate the delivery of recycling T-cell receptors to the immune synapse. *J. Cell Sci.* 128: 2541–2552.
18. Vivar, O. I., G. Masi, J. M. Carpier, J. G. Magalhaes, D. Galgano, G. J. Pazour, S. Amigorena, C. Hivroz, and C. T. Baldari. 2016. IFT20 controls LAT recruitment to the immune synapse and T-cell activation in vivo. *Proc. Natl. Acad. Sci. USA* 113: 386–391.
19. Martín-Cófreces, N. B., F. Baixauli, M. J. López, D. Gil, A. Monjas, B. Alarcón, and F. Sánchez-Madrid. 2012. End-binding protein 1 controls signal propagation from the T cell receptor. *EMBO J.* 31: 4140–4152.
20. Wandinger-Ness, A., and M. Zerial. 2014. Rab proteins and the compartmentalization of the endosomal system. *Cold Spring Harb. Perspect. Biol.* 6: a022616.
21. Welz, T., J. Wellbourne-Wood, and E. Kerkhoff. 2014. Orchestration of cell surface proteins by Rab11. *Trends Cell Biol.* 24: 407–415.
22. van Ijzendoorn, S. C. 2006. Recycling endosomes. *J. Cell Sci.* 119: 1679–1681.
23. Heider, M. R., and M. Munson. 2012. Exorcising the exocyst complex. *Traffic* 13: 898–907.

24. Horgan, C. P., and M. W. McCaffrey. 2009. The dynamic Rab11-FIPs. *Biochem. Soc. Trans.* 37: 1032–1036.
25. Horgan, C. P., S. R. Hanscom, E. E. Kelly, and M. W. McCaffrey. 2012. Tumor susceptibility gene 101 (TSG101) is a novel binding-partner for the class II Rab11-FIPs. *PLoS One* 7: e32030.
26. Jing, J., J. R. Junutula, C. Wu, J. Burden, H. Matern, A. A. Peden, and R. Prekeris. 2010. FIP1/RCP binding to Golgin-97 regulates retrograde transport from recycling endosomes to the trans-Golgi network. *Mol. Biol. Cell* 21: 3041–3053.
27. Wilson, G. M., A. B. Fielding, G. C. Simon, X. Yu, P. D. Andrews, R. S. Hames, A. M. Frey, A. A. Peden, G. W. Gould, and R. Prekeris. 2005. The FIP3-Rab11 protein complex regulates recycling endosome targeting to the cleavage furrow during late cytokinesis. *Mol. Biol. Cell* 16: 849–860.
28. Schindelin, J., I. Arganda-Carreras, E. Frise, V. Kaynig, M. Longair, T. Pietzsch, S. Preibisch, C. Rueden, S. Saalfeld, B. Schmid, et al. 2012. Fiji: an open-source platform for biological-image analysis. *Nat. Methods* 9: 676–682.
29. Costes, S. V., D. Daelemans, E. H. Cho, Z. Dobbin, G. Pavlakis, and S. Lockett. 2004. Automatic and quantitative measurement of protein-protein colocalization in live cells. *Biophys. J.* 86: 3993–4003.
30. Kao, J. P., A. T. Harootunian, and R. Y. Tsien. 1989. Photochemically generated cytosolic calcium pulses and their detection by fluo-3. *J. Biol. Chem.* 264: 8179–8184.
31. Antón, O. M., L. Andrés-Delgado, N. Reglero-Real, A. Batista, and M. A. Alonso. 2011. MAL protein controls protein sorting at the supramolecular activation cluster of human T lymphocytes. *J. Immunol.* 186: 6345–6356.
32. Horgan, C. P., S. R. Hanscom, R. S. Jolly, C. E. Futter, and M. W. McCaffrey. 2010. Rab11-FIP3 links the Rab11 GTPase and cytoplasmic dynein to mediate transport to the endosomal-recycling compartment. *J. Cell Sci.* 123: 181–191.
33. Straus, D. B., and A. Weiss. 1992. Genetic evidence for the involvement of the lck tyrosine kinase in signal transduction through the T cell antigen receptor. *Cell* 70: 585–593.
34. Nika, K., C. Soldani, M. Salek, W. Paster, A. Gray, R. Etzensperger, L. Fugger, P. Polzella, V. Cerundolo, O. Dushek, et al. 2010. Constitutively active Lck kinase in T cells drives antigen receptor signal transduction. *Immunity* 32: 766–777.
35. Bouchet, J., I. Del Río-Iñiguez, R. Lasserre, S. Agüera-Gonzalez, C. Cuche, A. Danckaert, M. W. McCaffrey, V. Di Bartolo, and A. Alcover. 2016. Rac1-Rab11-FIP3 regulatory hub coordinates vesicle traffic with actin remodeling and T-cell activation. *EMBO J.* 35: 1160–1174.
36. Maxfield, F. R., and T. E. McGraw. 2004. Endocytic recycling. *Nat. Rev. Mol. Cell Biol.* 5: 121–132.
37. Weissman, A. M., S. J. Frank, D. G. Orloff, M. Merćep, J. D. Ashwell, and R. D. Klausner. 1989. Role of the zeta chain in the expression of the T cell antigen receptor: genetic reconstitution studies. *EMBO J.* 8: 3651–3656.
38. D'Oro, U., M. S. Vacchio, A. M. Weissman, and J. D. Ashwell. 1997. Activation of the Lck tyrosine kinase targets cell surface T cell antigen receptors for lysosomal degradation. *Immunity* 7: 619–628.